applied sciences

MDPI

Article

Ground Settlement of Deeply Buried Two-Lane Tunnels with Large Cross-Sections Using Different Construction Methods

Yugang Han [1,2], Changming Wei [1,2], Mengyuan Cui [1,*], Hong Xie [1,3], Yangwang Ou [1,3], Hao Zhu [1,2] and Taoying Liu [1,2,3,*]

[1] School of Resources & Safety Engineering, Central South University, Changsha 410083, China
[2] Guangxi Liubin Expressway Construction and Development Co., Ltd., Nanning 530023, China
[3] Hunan Lianzhi Technology Co., Ltd., Changsha 410200, China
* Correspondence: 215511013@csu.edu.cn (M.C.); taoying@csu.edu.cn (T.L.); Tel.: +86-151-1112-0528 (T.L.)

Abstract: To ensure the safety of excavations such as large section tunnels of the Guangxi Liubin Highway Tunnel Project, we implemented a simulation analysis of 3D tunnel models based on finite software for different construction methods. Different from the traditional simulation, this paper uses various construction methods to compare, study, and analyze the advantages and disadvantages of different excavation methods by combining them with the excavation. The feasibility of different construction methods was analyzed by studying the mechanical characteristics and settlement changes using the Cross Diaphragm (CRD), Center Diaphragm (CD), and full-section methods while building a large section tunnel. The arch perimeter deformation and surface settlement during the initial support and secondary lining proved that the CRD excavation method is the most favorable and causes the least damage to the stability of the surrounding rock. For the analysis of surface subsidence, the "V"-shaped surface subsidence curve excavated by the CRD method is the closest to the subsidence curve. However, we used the adjusted peak formula to fit the prediction formula for the surface settlement curve of the deep-buried two-lane tunnel with a large cross-section applicable to this project, which will provide an important reference for similar projects.

Keywords: CRD method; CD method; full-section method; surface settlement; large-section tunnel

check for updates

Citation: Han, Y.; Wei, C.; Cui, M.; Xie, H.; Ou, Y.; Zhu, H.; Liu, T. Ground Settlement of Deeply Buried Two-Lane Tunnels with Large Cross-Sections Using Different Construction Methods. *Appl. Sci.* **2022**, *12*, 11105. https://doi.org/10.3390/app122111105

Academic Editor: Arcady Dyskin

Received: 28 August 2022
Accepted: 17 October 2022
Published: 2 November 2022

Publisher's Note: MDPI stays neutral with regard to jurisdictional claims in published maps and institutional affiliations.

Copyright: © 2022 by the authors. Licensee MDPI, Basel, Switzerland. This article is an open access article distributed under the terms and conditions of the Creative Commons Attribution (CC BY) license (https://creativecommons.org/licenses/by/4.0/).

1. Introduction

With the proposal of the "One Belt, One Road" plan of China, Guangxi province continues to consider transportation development as a priority, and the construction of transport was continuously hastened. Since the construction of the first high-speed railroad in Guangxi Province in 1997, the expressways in this province have reached 6803 km, and a complex and vast network of highways was built, which has improved the transport capacity. It is necessary to construct highway tunnels for expressways, although different construction methods will have different effects on tunnel construction. Huang et al. [1] compared different construction methods. They also analyzed the stability evolution of different parts of highway tunnel construction and the settlement changes of performing railway tunnels caused by new highway tunnels passing through existing railway tunnels. Cui et al. [2] used the FLAC 3D limited software to carry out a three-dimensional numerical simulation of the tunnel excavation with four construction methods; however, they analyzed the mechanical response law of the rock and supporting structure around the tunnel for various construction methods. Wang et al. [3] carried out numerical simulations using the MIDAS finite software. They analyzed and studied the displacement and stress characteristics of double-arch tunnels for different construction methods. Yu et al. [4] studied the changes in stress and strain during the construction of double-arch tunnels by analyzing different construction methods. Zhang et al. [5] studied and analyzed the mechanical behavior of rocks during tunnel construction under different schemes by numerical analysis. Wu et al. [6] studied tunnel deformation, track settlement, and construction reasons.

With the help of numerical simulation software, it is possible to predict the problems faced during the tunnel excavation project, not only for reference purposes but also to predict, in advance, the various problems that may arise during the excavation, such as over-excavation, stress concentration, and excessive deformation around the hole [7–9]. Thus, the project [10–12] successfully reduced the number of issues and difficulties faced. The ground settlement caused by the tunnel excavation often leads to damage or destruction of ground buildings, and various numerical analysis methods are used to simulate the effects of ground settlement, to better protect the ground buildings and reduce unnecessary economic losses [13–15].

The tunnel excavation will cause a certain surface settlement. This settlement is more complex after the double tunnel excavation. The surface settlement during tunnel excavation mainly contains single tunnel surface settlement, double tunnel surface settlement, shallow-buried layer surface settlement, and deep-buried layer surface settlement [13,16–18]. The study of the surface settlement is critical because constructing tunnels will cause some damage to the buildings [19–21], and the study of settlement plays a crucial role in excavating tunnels and protecting buildings.

In this paper, based on Gaoliang Tunnel in Guangxi province, constructing the CD, CRD, and full-section methods were analyzed using the finite software. The tunnel vault displacement, deformation around the tunnel, the stress of the initial support and secondary lining, and the law of surface settlement during excavation of deep-buried separate large-section tunnels were studied for different construction methods [22–25]. However, the tunnel influence law of large section split tunnel excavation was studied by comparing the simulation results with the surveying data. Finally, the prediction formula of the surface settlement curve of the large-section deep-buried double-track tunnel suitable for this project is fitted, which provides an important theoretical basis for similar projects.

2. Project Overview

The entrance of the Gaoliang Tunnel is located on the northeast side of Gaoliang Village in Nanning City, and the exit is located on the southwest side of Tanchong Village in Chenping Town. It is a split double-hole tunnel. The starting and ending mileage of the left side is ZK32 + 647.00~ZK34 + 955.00, and the maximum buried depth is nearly 374 m. The starting and ending mileage on the right side is K32 + 636.00~K34 + 917.00, and the maximum buried depth is nearly 378 m. The project map is shown in Figure 1.

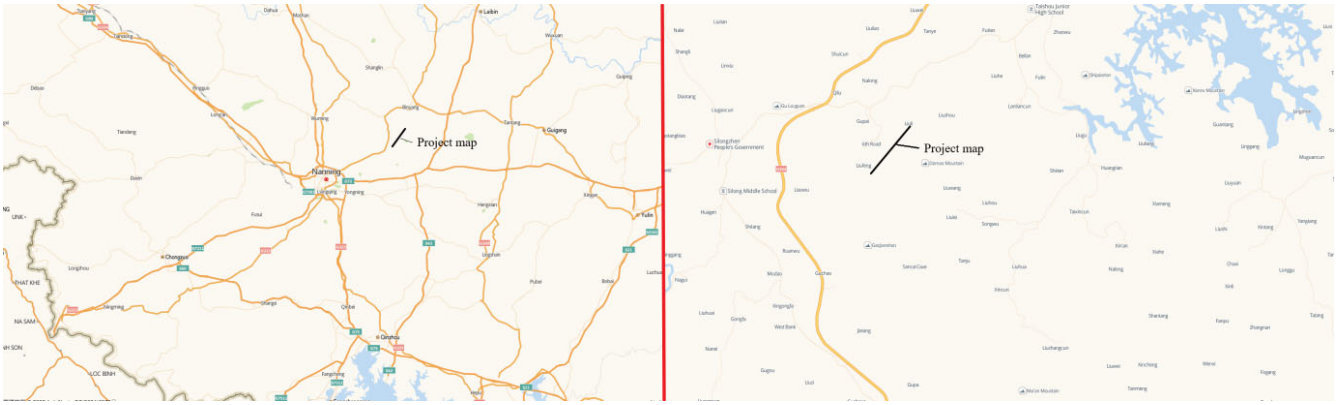

(**a**) (**b**)

Figure 1. Project Location map. (**a**) Large map. (**b**) Mini map.

According to the construction design, this paper tackles the right line K34 + 620–K34 + 680 and the matching left line. Each line is 60 m, a section width of 12.02 m, and a height of 8.53 m. The details of the tunnel are shown in Figure 2. The International Tunneling Association's guidance for judging large cross-sections is shown in Table 1. The distance between the two tunnels is 20 m, and the buried depth of the simulated part is 95.31 m.

From top to bottom, the soil layers in the tunnel section are fully weathered broken rock, strongly differentiated rock, and moderately weathered rock. The surrounding rock of the buried tunnel is grade V, and the CRD, CD, and full-section methods are used for construction, while small, advanced conduits are used for advanced support. The shotcrete, steel mesh, and anchor are used as initial support. A waterproof layer is set up, and secondary lining and bottoming are then performed.

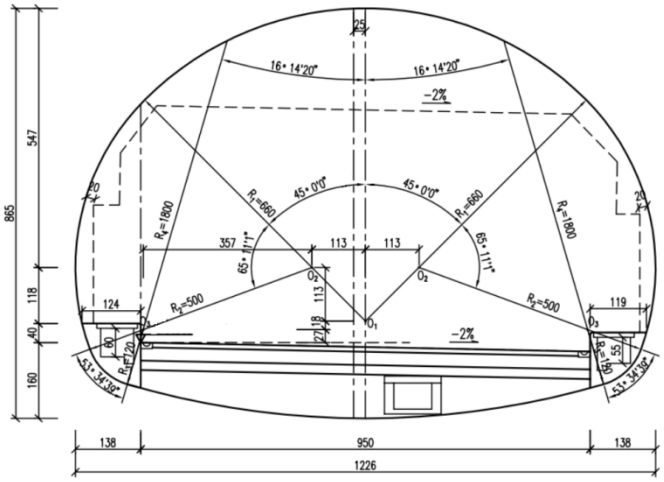

Figure 2. Tunnel excavation section size drawing.

Table 1. Judgment criteria of the International Tunnelling Association for cross-sections.

Grade Classification	Clearance Cross-Sectional Area (m^2)
Ultra-small cross-section	<3.0
Small cross-section	3.0–10.0
Medium cross-section	10.0–50.0
Large cross-section	50.0–100.0
Extra large cross-section	>100.0

Full-section construction method:

In this method, the tunnel section is excavated and formed at one time, and the lining is then supported. This method reduces the number of excavations by reducing the disturbance to the surrounding rocks, which is convenient for construction and conducive to protecting the natural bearing capacity of the surrounding rocks but has relatively high needs on lithology.

CD construction method [26]:

The CD method is also known as the middle partition method. One side of the tunnel is first excavated, the middle part of the design is used as the middle partition, and the other side is then excavated. It is mainly used in the double-track tunnel IV, deep-buried hard rock section, and old loess tunnel section (with grade IV surrounding rock).

CRD construction method [27]:

This method is also referred to as the cross-septum method. It is mainly used for large-section tunnel excavation. It is followed by the excavation and support of tunnel ②, tunnel ③, and tunnel ④ in sequence.

The excavation sequence is shown in Figure 3. Tunnel ② is first excavated, followed by the initial support and inner support. The excavation and support of tunnel ②, tunnel ③, and tunnel ④ are then carried out in sequence.

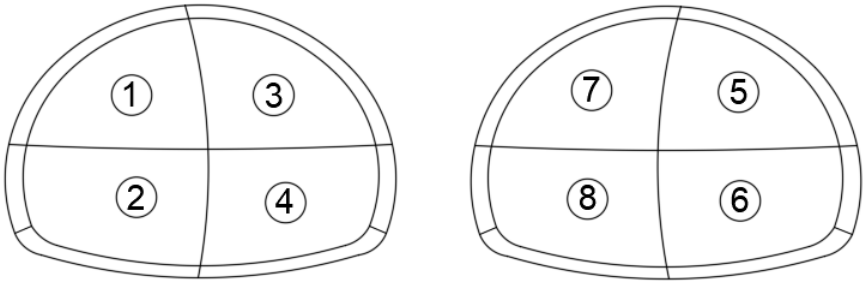

Figure 3. Separate tunnel excavation sequence diagram.

3. Model Building

The split tunnel model shown in Figure 3 was constructed to analyze the mechanical properties and deformation characteristics of the large section split tunnel during construction. Considering the numerical simulation accuracy, the surrounding rock on the left and right sides of the tunnel is greater than five times the width of the tunnel diameter, and the surrounding rock at the lower part of the tunnel is greater than five times the height of the tunnel diameter. The size of the final model is 180 m × 60 m × 175 m. In the model, the surrounding rock part and the secondary lining part are solid, and the Moore–Coulomb constitutive model is used. The initial support and inner support are simulated by a plate, the anchor rod is simulated by a one-dimensional implanted truss, and they are all simulated by the elastic constitutive model. The mesh construction uses a hybrid tetrahedral mesh, the model boundary is automatically constrained, and the self-weight is set at the same time. These material boundaries were obtained from experiments. The specific data are shown in Table 2. We also use the international classification to classify the rocks [28]. The CRD, CD, and full-section methods are used to simulate constructing the tunnel. The construction and surveying data are analyzed and compared, and the mechanical properties and deformation characteristics of different construction methods are studied. The final built model contains 100,000 grid cells, as shown in Figure 4.

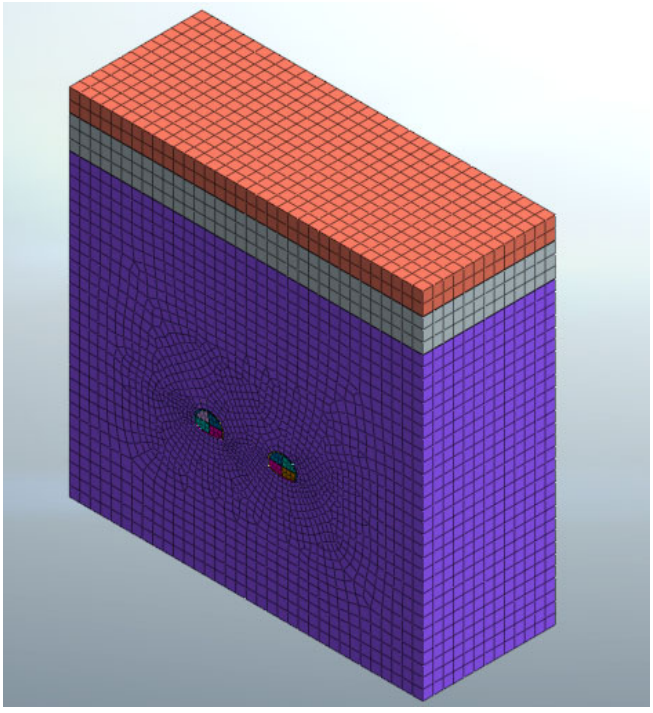

Figure 4. Separate tunnel model.

Table 2. Material physical and mechanical parameters.

Material Properties	Test Weight γ/KN·m^{-3}	Elastic Modulus E/MPa	Poisson's Ratio μ	Cohesion c/KPa	Internal Friction Angle φ/°
Fully weathered crushed rock	19.7	7	0.3	12.6	16.2
Strongly weathered rock	23	500	0.3	20	33
Medium weathered rock	25	2000	0.25	200	35
Initial support	24	15,000	0.2	/	/
Secondary lining	22	31,500	0.3	/	/
Anchor	78.5	210,000	0.3	/	/

4. Analysis of the Tunnel Construction Simulation Results

4.1. Surveying Point Layout

To measure the deformation of the surrounding rock of the tunnel during the tunnel construction, four surveying points are set up on each tunnel boundary, and one set of surveying points is set every 20 m, for four sets of surveying points [6]. Similarly, after excavating the left tunnel is completed, excavating the right tunnel is performed. The sequence and steps are symmetrical with those of the left side. Four groups of surveying points are also set and four surveying points are set in each group to survey the tunnel arch during the tunnel excavation. The surveying point layout showing the top subsidence, tunnel perimeter convergence, and the arch bottom bulge is presented in Figure 5.

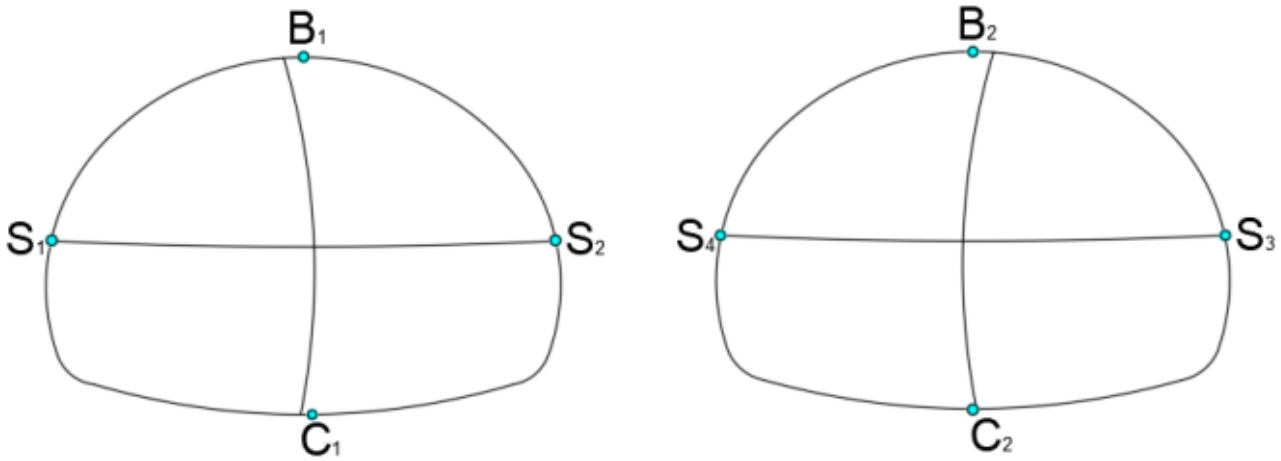

Figure 5. Layout drawing of the separated tunnel surveying points.

4.2. Vault Settlement and Tunnel Perimeter Convergence

The deformation surveying is carried out in the left tunnel and the right tunnel, and the deformation curve of each surveying point is obtained by analyzing the simulation results. B1 and B2 are the surveying points at the top of the tunnel, and S1, S2, S3, and S4 are the surveying points for the horizontal convergence of the tunnel. Data analysis is performed on the deformation around the tunnel at 0 m, 20 m, 40 m, and 60 m. The simulation at 0 m represents the tunnel opening excavation. The simulation at 20 m and 40 m represents the excavation process in the middle of the tunnel, and the simulation at 60 m represents the excavation at its end. The deformation curves of each surveying point of different excavation methods are obtained (Figure 6). It can be deduced that the roof subsidence is negative, and the horizontal convergence around the hole is also negative.

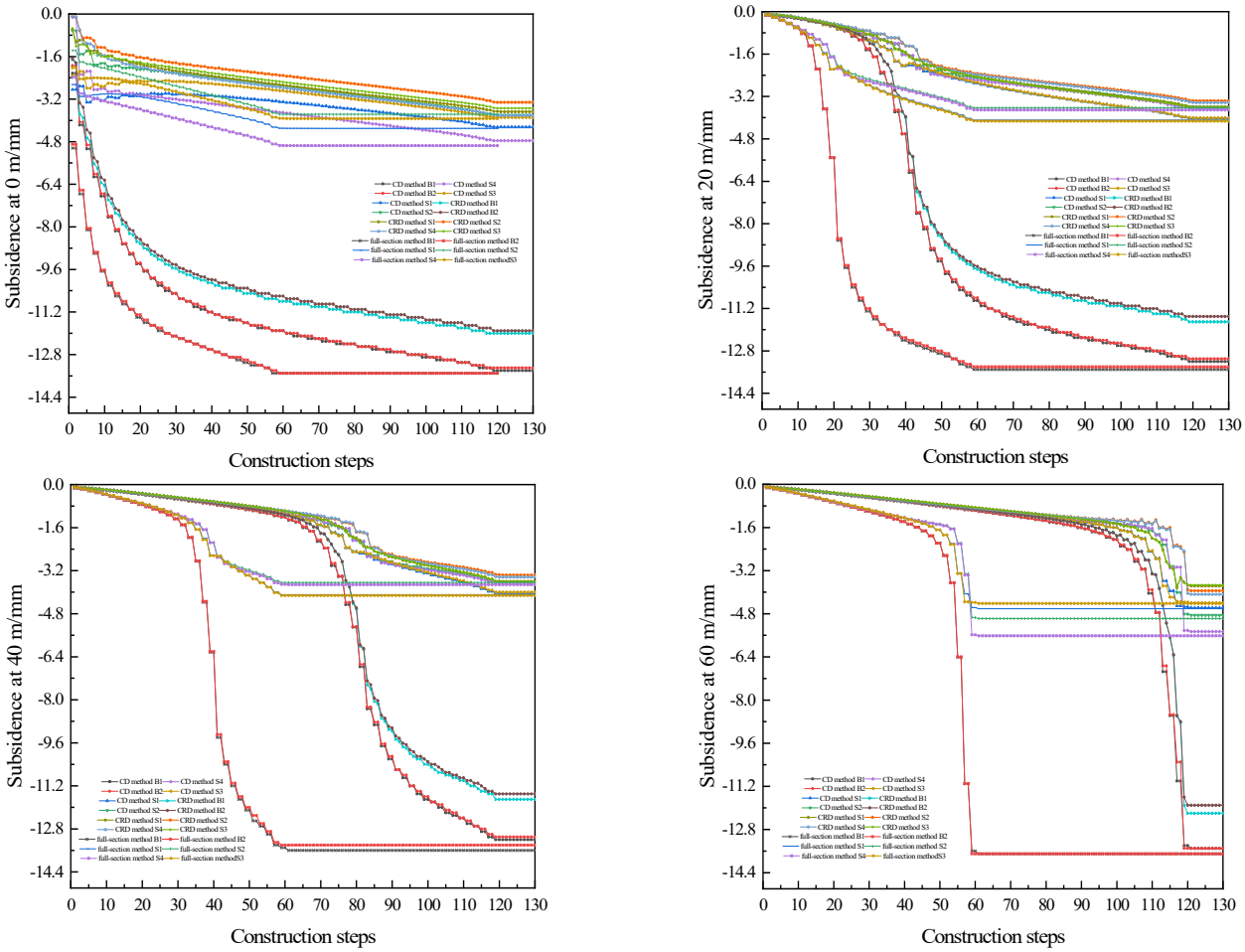

Figure 6. Deformation diagram of tunnels with different excavation methods.

It can be seen from Figure 6 that the full-section method is the fastest one, and the CD and CRD methods have the same construction speed. The shapes of the vault settlement curves surveyed at different positions are different. More precisely, the surveying curve at 0 m is an inverse curve, while the settlement curves surveyed at 20 m, 40 m, and 60 m are first gentle, then sharp, and finally flattened. The curve at 60 m has the largest deformation rate because the deformation curve at the end of the tunnel excavation is simulated at 60 m. The settlement curve of the full-section method has the largest slope, and it is the most difficult to support, while the CD and CRD methods have relatively gentle settlement curves, which are relatively easy to support and the most favorable for the overall maintenance of the tunnel. The CRD excavation method has the smallest settlement, which presents its largest advantage. It is the most complicated in construction and excavation but the most favorable for the stability of the surrounding rock around the tunnel. The full-section method excavates the entire tunnel section, the stability of the surrounding rock is the most difficult to control, and the settlement is the largest.

Through the analysis of the tunnel settlement map of different excavation methods, it is found the position of the maximum settlement of the vault occurs in the excavation of the full-section method, and the maximum settlement value is 13.7 mm. After the first part of the tunnel was excavated, the maximum settlement of the vault reached 5.04 mm, which accounts for 36.79% of the total settlement. When excavating 10 m back from the surveying point, the maximum settlement of the vault reached 11.3 mm, the settlement increased by 45.69%, and the stability of the surrounding rock was destroyed the most. The CRD method has the smallest excavation settlement of 12.2 mm. After the first part of the tunnel excavation, settling the tunnel vault reaches 1.74 mm, which accounts for

14.26% of the total settlement. After excavating 10 m back from the surveying point, the maximum settlement of the vault increased by 4.21 mm, and the settlement increased by 34.49%, which had the least impact on the stability of the surrounding rock.

According to Table 3, the settlement of the vault is much larger than the horizontal convergence around the tunnel. The maximum settlement value during the excavation of the CRD method reached 12.2 mm, which appeared at the B1 position of the 60 m surveying point. The maximum settlement value during the excavation of the CD method reached 13.5 mm, which also appeared at the B1 position of the 60 m surveying point. For the full-section method, during the excavation, the maximum settlement value reached 13.7 mm, which also appeared at the 60 m surveying point B1. It can be seen from the vault settlement the CRD method has the smallest maximum settlement value, the full-section method has the largest settlement value, and the settlement value of the CD method is in the middle, which appears at the position of the 60 m surveying point S4. During the excavation of the CD method, the maximum horizontal convergence is 5.46 mm, which also appears at the 60 m surveying point S4. The maximum horizontal convergence during the excavation of the full-section method is 5.62 mm, which also appears at the 60 m surveying point S4. After analyzing the settlement value of each surveying point, it can be concluded the full-section excavation method has the lowest stability of surrounding rock, and the CRD method has the highest surrounding rock stability.

Table 3. Maximum deformation value of surveying points in different excavation methods.

Excavation Method/Surveying Point Location/Maximum Deformation (mm)		Surveying Point at 0 m	Surveying Point at 20 m	Surveying Point at 40 m	Surveying Point at 60 m
CRD method	B1	−12.0	−11.7	−11.7	−12.2
	C1	12.6	11.8	11.6	12.0
	B2	−11.9	−11.5	−11.5	−11.9
	C2	12.6	11.8	11.6	12.0
	S1	−3.67	−3.6	−3.6	−3.7749
	S2	−3.32	−3.36	−3.36	−3.94754
	S3	−3.54	−3.62	−3.61	−3.73523
	S4	−3.81	−3.43	−3.44	−4.07924
CD method	B1	−13.4	−13.2	−13.2	−13.5
	C1	13.9	13.3	13.1	13.2
	B2	−13.3	−13.1	−13.1	−13.5
	C2	13.9	13.3	13.1	13.2
	S1	−4.25	−4.02	−4.04	−4.58
	S2	−3.79	−3.59	−3.6	−4.85
	S3	−3.89	−4.01	−4	−4.4
	S4	−4.76	−3.66	−3.66	−5.46
Full-section method	B1	−13.5	−13.5	−13.6	−13.7
	C1	14.1	14.1	13.9	13.4
	B2	−13.5	−13.4	−13.4	−13.7
	C2	14.1	14.1	13.9	13.5
	S1	−4.3	−4.09	−4.11	−4.61
	S2	−3.77	−3.63	−3.64	−4.98
	S3	−3.93	−4.13	−4.12	−4.42
	S4	−4.95	−3.71	−3.72	−5.62

4.3. Deformation of Arch Bottom

During the tunnel excavation, a deformation will occur around the entire tunnel. Table 3 shows the maximum deformation values of all the surveying points. The maximum deformation of the vault, the vault bottom, and the spandrel are recorded. The maximum deformation is not the vault deformation. The deformation of the bottom of the tunnel is larger. The deformation diagram of the bottom of the arch with different excavation methods is shown in Figure 7.

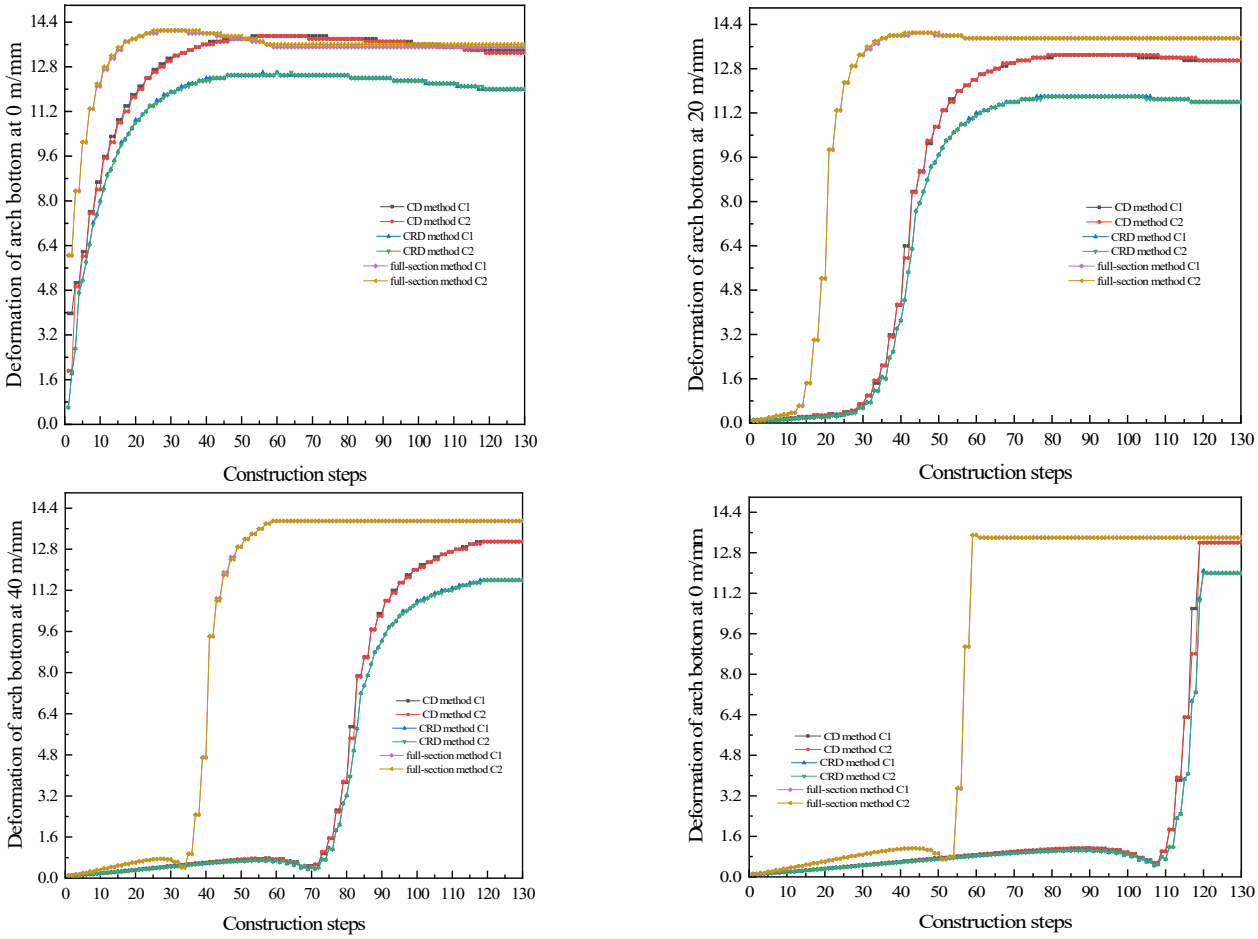

Figure 7. Deformation diagram of the arch bottom with different excavation methods.

It can be seen from Table 3 that the deformation at the top and bottom of the tunnel is much larger than that around the tunnel. During the excavation of the CRD method, the maximum uplift value reached 12.6 mm, which appeared at the 0 m surveying point C1, and this was not the final deformation. After a certain construction time, the deformation value rebounded, and the maximum rebound value was 0.6 mm. During the whole CRD excavation, the deformation curve detected at 0 m is similar to the inverse curve, but as it progresses, the deformation value rebounds and finally stabilizes at 12.0 mm. The main reason for this behavior is that in the excavation process, the in situ stress is broken and reorganized, which will have a certain impact on the surrounding rock. In addition, although the tunnel is supported, the stress of the surrounding rock will cause the tunnel to be damaged over time, and therefore a slow deformation occurs. The maximum uplift value in the CD method excavation reached 13.9 mm, which is also consistent with the CRD method excavation process. The maximum uplift value is not the final deformation value, and the maximum rebound value is 0.6 mm. During the excavation of the full-section method, the maximum uplift value reached 14.1 mm, and the rebound also occurred with a maximum value of 0.5 mm. The largest arch bottom deformation occurs in the full-section excavation, which also has the highest deformation speed, and the maximum uplift value at the 20 m surveying points C1 and C2 is 14.1 mm.

By analyzing Figures 6 and 7, it can be deduced that in vault settlement, horizontal convergence of the tunnel circumference, and deformation of the tunnel bottom, CRD is the most decent excavation method. The tunnel deformation rate of the CD method is not much different from that of the full-section method. The full-section method has the largest deformation around the tunnel and the largest deformation rate; therefore, CRD excavation is the most decent for large-section tunnel excavation in tunnel settlement and deformation.

4.4. Analysis of Initial Support Force

The analysis of the three excavation methods shows the initial support stress is the smallest during the excavation of the CRD method, where the maximum tensile stress is 1.05329 MPa, and the maximum compressive stress is −25.5873 MPa. See Table 4 for details. The support force is then analyzed. By comparing the maximum and minimum principal stress of the initial support of the three excavation methods, it is deduced the full-section method has the largest initial support force while the CRD method has the smallest one. The minimum and maximum compressive stress values on the initial support of the CRD method are 0.86 and 0.927 times those of the full-section method, respectively. Figure 8 shows the initial support stress nephogram of the CRD method excavation. A small difference exists between the initial support stress nephograms of the three excavation methods, but the maximum tensile and compressive stress values are different, and the force distribution is roughly the same; therefore, only the initial support force cloud map of the CRD method is analyzed. It can be seen from Figure 8 that in the maximum principal stress diagram, the main tensile stress is distributed at the top and bottom of the vault, while the compressive stress is mainly distributed on both sides of the tunnel. In addition, the maximum tensile stress is 1.05329 MPa and the maximum compressive stress is −10.2049 MPa. In the minimum principal stress diagram, there is only compressive stress, but the compressive stress received by the top and bottom of the vault is much smaller than that on the two sides of the tunnel. The maximum compressive stress is −25.5873 MPa and the minimum compressive stress is −3.57857 MPa.

Table 4. Initial support force.

Initial Support Force		CRD Method	CD Method	Full-Section Method
Maximum principal stress (MPa)	MAX	1.05329	1.37031	−1.66592
	MIN	−10.2049	−10.9626	−11.1948
Minimum principal stress (MPa)	MAX	−3.57857	−3.98357	−4.15936
	MIN	−25.5873	−27.0095	−27.5909

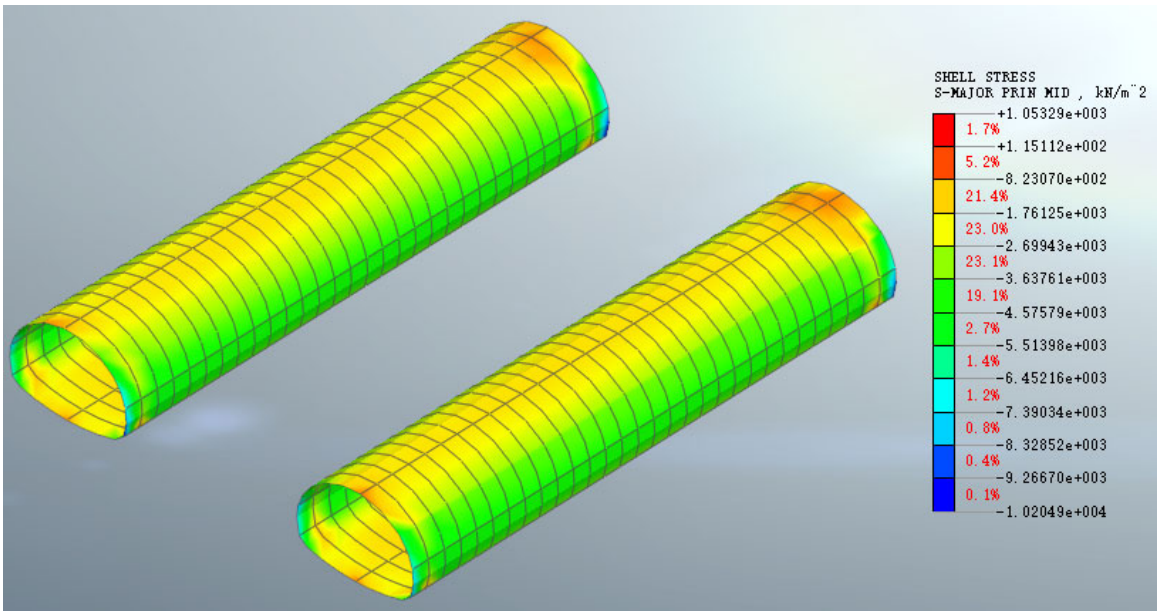

(**a**)

Figure 8. *Cont.*

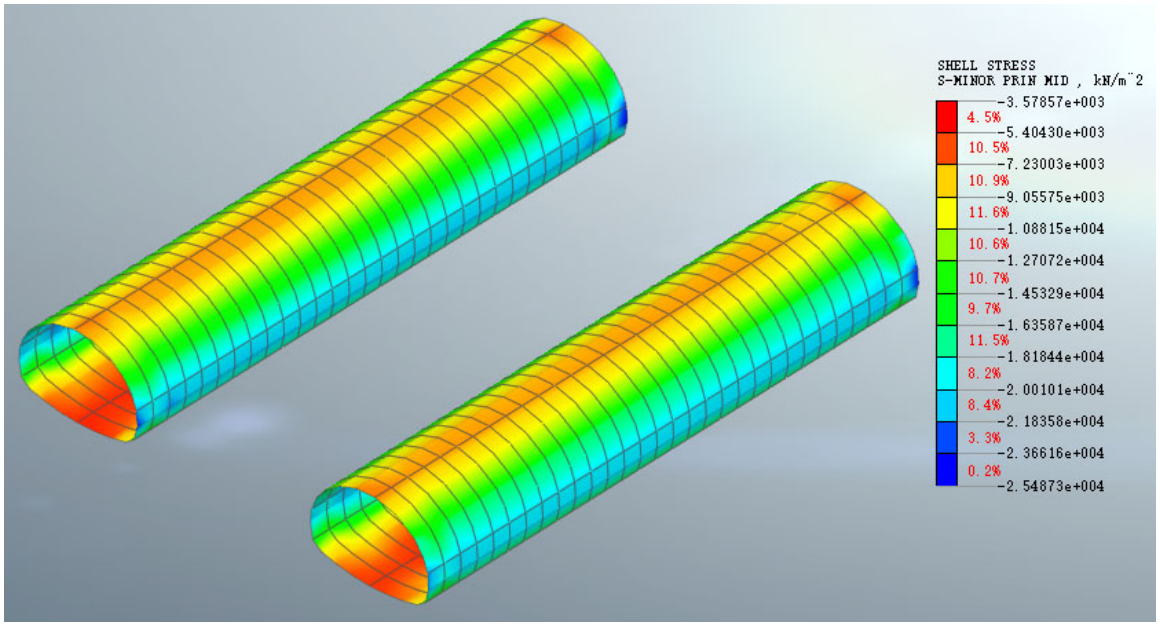

(**b**)

Figure 8. The initial support maximum and minimum stress clouds for the CRD method. (**a**) Maximum principal stress by the CRD method. (**b**) Minimum principal stress by the CRD method.

4.5. Force Analysis of Secondary Lining

After the initial support is completed, the deformation of the surrounding rock is stable, and the secondary lining is applied when the initial support is fully stressed. Eight surveying points were selected for settlement surveying, and the selected locations are similar to the tunnel settlement surveying points. The main stress is similar to that of the initial support; however, due to the effect of the initial support, a part of the surrounding rock stress has been reduced, and therefore the surrounding rock pressure of the secondary lining support will be reduced. It can be observed from Figures 9 and 10 that the deformation law of the secondary lining is roughly the same for the three excavation methods; therefore, only the deformation of the secondary lining during the excavation of the CRD method is analyzed. The specific deformation data are shown in Table 5. In the CRD excavation method, the deformation of the secondary lining is the smallest, the maximum settlement of the arch bottom of the secondary lining is 11.33806 mm, the maximum horizontal convergence around the hole is 4.013874 mm, and the maximum deformation of the arch bottom is 11.3943 mm. Figure 11 shows the stress of the secondary lining during CRD excavation. The maximum plastic strain is distributed on both sides of the tunnel, especially inside the tunnel. The numerical simulation results show the maximum tensile stress is also distributed on both sides of the secondary lining, while the maximum compressive stress is distributed on the top and bottom of the secondary lining. It can be seen from the deformation comparison diagram of the secondary lining of the three excavation methods the deformation trend is consistent with that of the tunnel vault; however, the maximum deformation of each surveying point is slightly smaller than that of the tunnel vault. The deformation value of the CRD method is the smallest, and its deformation rate is the slowest. The deformation value of the full-section method is the largest, and its deformation rate is the fastest.

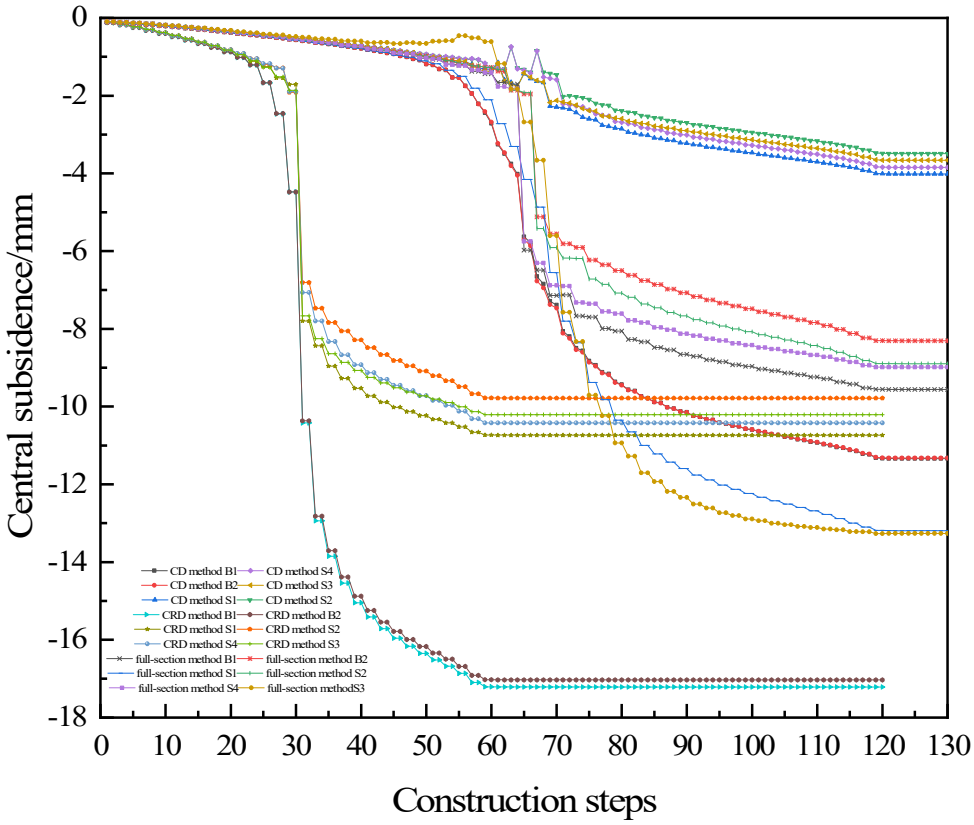

Figure 9. Settlement diagram of the secondary lining arch.

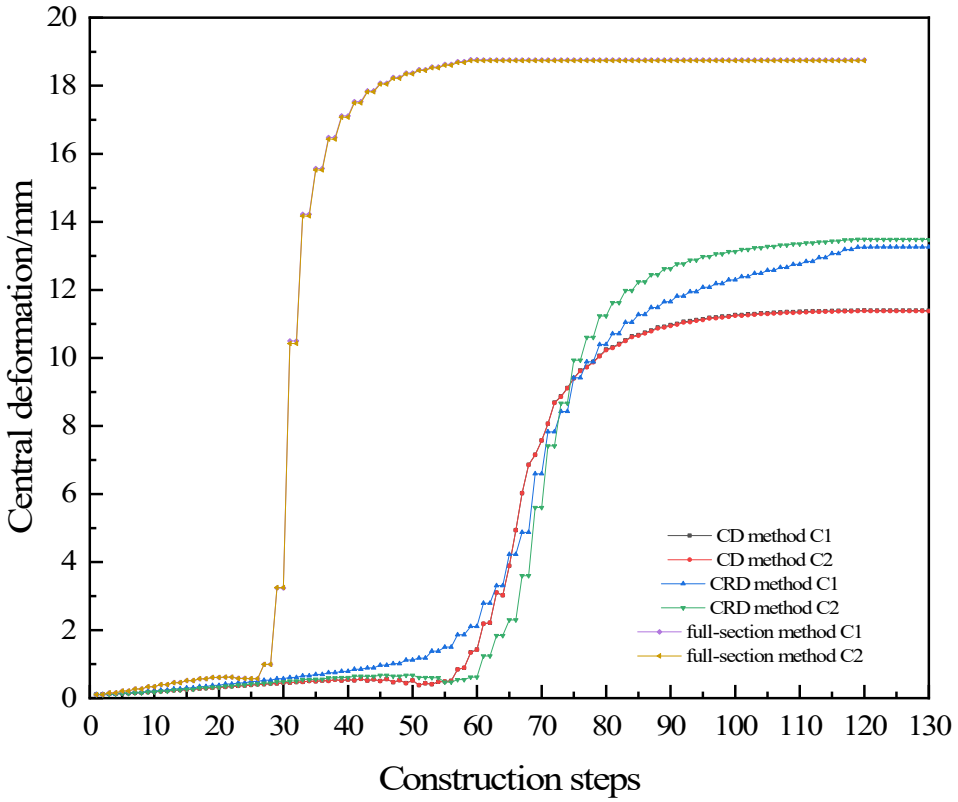

Figure 10. Deformation diagram of the secondary lining arch bottom.

Table 5. Deformation of secondary lining with different excavation methods.

Surveying Point/Displacement (mm)/Excavation Method	CRD Method	CD Method	Full-Section Method	Surveying Point/Displacement (mm)/Excavation Method	CRD Method	CD Method	Full-Section Method
C1	11.3943	13.26114	18.76242	S1	−4.013874	−13.19124	−10.73508
C2	11.3758	13.48232	18.73647	S2	−3.489805	−8.898034	−9.782638
B1	−11.33806	−9.560629	−17.21646	S3	−3.663354	−13.26354	−10.20903
B2	−11.32381	−8.305074	−17.03111	S4	−3.844614	−8.985437	−10.42312

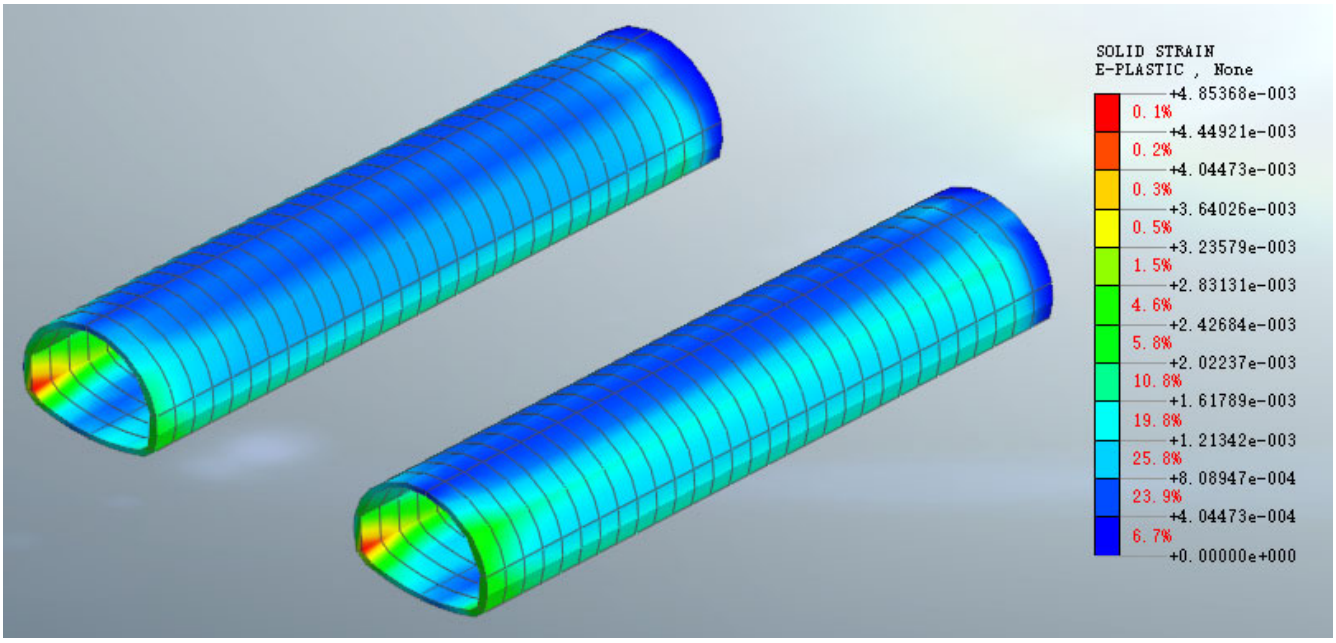

Figure 11. Effective plastic strain of secondary lining by the CRD method.

5. Surface Subsidence Model Optimization

5.1. Subsidence Surveying

The tunnel construction has a certain impact on the surface, causing problems such as surface subsidence. In this section, the surface subsidence survey during the excavation of the split tunnel is carried out. The detection position is the model center line. The influence of the three construction methods on the surface after excavation is analyzed and compared with the surveying data. The center line position of the surface surveying is shown in Figure 12, and the lateral layout of the surveying section is shown in Figure 13.

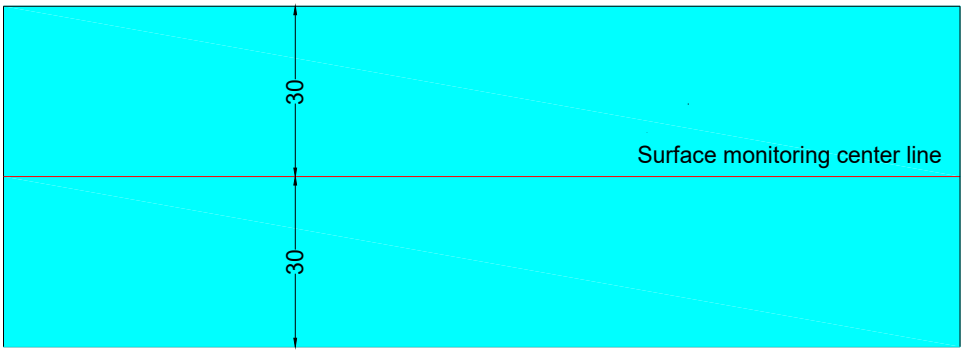

Figure 12. Location of the center line of the surface surveying.

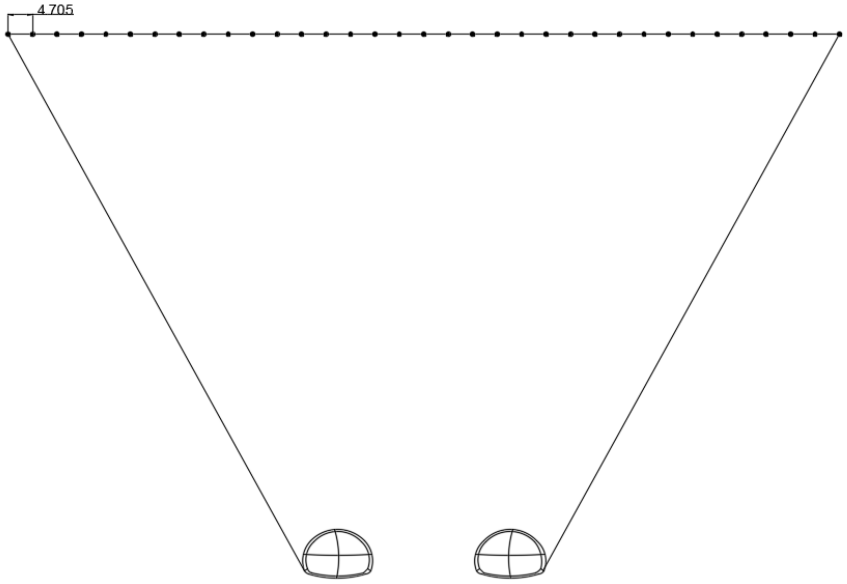

Figure 13. Schematic diagram of lateral arrangement of the surveying sections.

It can be seen from Figure 14 that the numerical simulation results are larger than the data, and the CRD method is the closest to the surveying data. It can be observed from the four surveying curves that the maximum settlement occurs at the midline position between the two tunnels, while the CRD method is the closest to the surveying data. Further, at the position beyond 65m from the center line, the settlement basically tends to be balanced. This position is located 40 m outside the left and right line tunnels, which is also the largest influence range of the double line tunnel. This is in line with the influence range of tunnel excavation (3–5 times the diameter of the tunnel). The CRD method has the smallest excavation settlement, and it is the closest to the actual settlement data. The CD and full-section methods mainly have the same settlement curves, and all the curves show a "V"-shaped settlement. The maximum settlement position appears at 4.85 m to the left of the midline. The maximum excavation settlements of the CRD, CD, and full-section methods are 7.27124 mm, 8.12842 mm, and 8.46477 mm, respectively. The maximum settlement value of the surveying data is 6.93465 mm. Compared with the other two excavation methods, the CRD method has certain advantages in terms of the surface settlement, which is not much different from the settlement. This is conducive to protecting ground buildings.

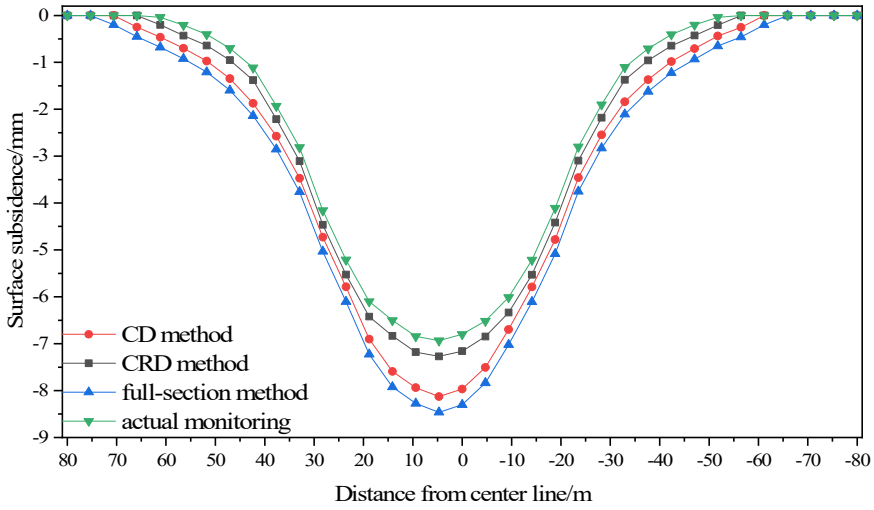

Figure 14. Surface surveying curve.

5.2. Classical Peck Model

Peck [29] deduced the lateral distribution of the surface settlement during the tunnel excavation is similar to the normal distribution curve and expressed the prediction formula of the surface settlement as:

$$S(x) = S_{max}\ (-\frac{x^2}{2i^2}) \tag{1}$$

where $S(x)$ is the surface settlement value at distance x from the central axis of the tunnel (m), i is the width coefficient of the surface settlement tank (m), S_{max} is the maximum subsidence of the ground at the centerline of the tunnel (m), and V_i is the soil loss rate, that is, the difference between the volume of the excavated soil during the tunnel construction and the volume of the completed tunnel. The volume of the completed tunnel includes the volume of pressed-in slurry wrapped around the tunnel.

Equation (1) presents the classic peak formula, and the model curve is "V" type, but some of the two-line tunnel settlement curves in the project are "W" type [30]. The shape of the ground subsidence curve should be related to the horizontal distance from the edge of the ground settlement tank to the tunnel axis, and the horizontal distance between the two tunnel axes. Whether two tunnels are close cannot be judged only based on the size of the horizontal distance between the two tunnel axes. Therefore, the shape of the ground subsidence curve caused by the double-line parallel excavation is related to the horizontal distance between the two tunnel axes, their buried depth, and the tunnel excavation radius. When the horizontal distance between the two tunnel axes is greater than the buried depth of the tunnel axis and the tunnel excavation radius, according to the geometrical principle, the land subsidence curve caused by the double-line parallel excavation will be distributed in a "W" shape [31]. In this project, due to the large burial depth, the horizontal distance between the two tunnel axes is much smaller than the buried depth of the tunnel axis and the tunnel excavation radius; therefore, the "V"-shaped settlement curve in this project conforms to the Peak curve needs.

5.3. Peak Formula for Two-Line Tunnel

(1) The study of peak on the Chicago two-lane tunnel shows settling the two-lane tunnel has a symmetrical distribution. In the settlement calculation, the double-track tunnel is replaced by a larger circle, and the radius of the large circle is given by:

$$R' = R + L/2 \tag{2}$$

where L is the distance between the two-track tunnel axes.

This method is a correction formula for symmetrical settlement. However, sometimes the surveying data are not symmetrical at the midline, and the maximum settlement value will deviate from the midline. In addition, this method has some limitations. In fact, for some of the buried depths, L is small. However, in some tunnels, a "W"-shaped settlement curve will appear, which does not satisfy the normal distribution in the peak formula.

(2) New et al. [32] modified the peak formula by considering the maximum land subsidence will be shifted and proposed the following calculation formula:

$$S(x) = \frac{\pi R^2 V_i}{i_t\sqrt{2\pi}} exp[-\frac{(x-a)^2}{2i_t^2}] \tag{3}$$

where i_t is the width coefficient of the surface settlement tank and a is the distance from the maximum value of the total settlement to the central axis of the two tunnels (m).

Equation (3) is then analyzed. Since this project tackles predicting the surface settlement of the double-track tunnel, the maximum settlement may not be on the central axis. In the measurement, the maximum settlement occurs at 4.85 m from the midline, the value of a is 4.85, and the radius of the tunnel is 12 m; therefore, in Equation (3), only two unknown coefficients (i.e., the total width coefficient of the surface settlement tank and the total soil loss rate) are required.

(3) GaussAmp model fitting.
It is expressed as:

$$y = y0 + A * exp[-0.5 * \left(\frac{x - x_c}{\omega}\right)^2] \quad (4)$$

where $y0$ is the GaussAmp model coefficient used to fit the maximum value of the data (the fixed value is 0), A is the GaussAmp model coefficient, which is related to the width coefficient of the surface settlement tank and the coefficient of soil loss rate, xc is the GaussAmp model coefficient, which is characterized by the distance the maximum value of total settlement deviates from the central axis of the two tunnels (equal to 4.85), and ω is the GaussAmp model coefficient characterizing the width coefficient of the surface settlement tank.

The fitting result stood after fitting the settlement values in this project according to Equation (4) is shown in Figure 15. The GaussAmp model is used as the fitting model. According to the surveying data in this project, the values of boundaries $y0$ and x_c are fixed. The maximum settlement of this project occurs at a position 4.85 m away from the midline, and the value of x_c is 4.85. The adjusted peak formula is used with $y0$ equal to 0. Fixed parameters and the data are fitted, and after many iterations, the fitting effect is finally achieved according to 35 sets of data. The values of A and ω are -7.29076 and 20.65042, respectively. By substituting these values in Equation (3), the stood value of V_i is -0.83422. In summary, the formula for the surface settlement of the double-track tunnel developed in this project is accurate.

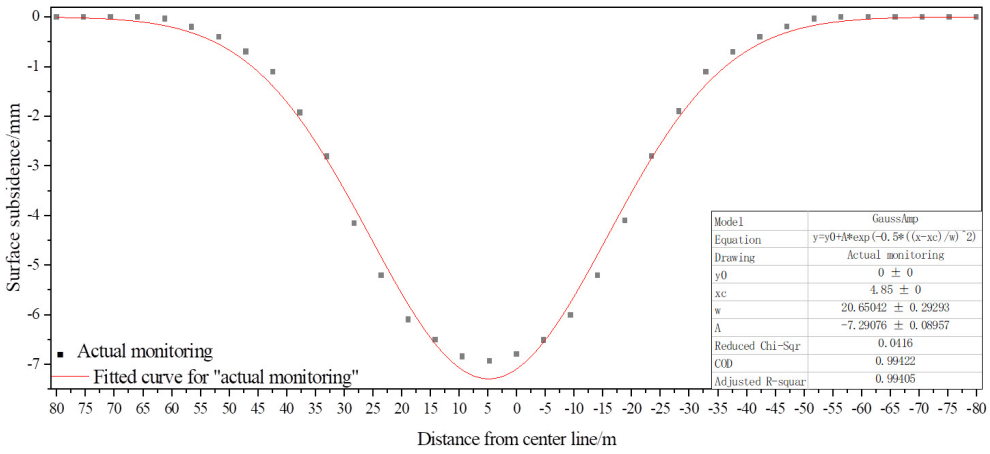

Figure 15. Settlement curve fitting.

6. Conclusions

(1) By analyzing the tunnel deformation maps of different excavation methods, it can be concluded that the CRD excavation method has the least effect on the convergence of the tunnel perimeter and is the most useful to the stability of the surrounding rock, so its surface settlement is also the smallest. In addition, the full-section method has the largest settlement and deformation and the greatest damage to the surrounding rock.

(2) Analysis of the support force. By comparing the maximum and minimum principal stress of the initial support of the three excavation methods, it is deduced that the full-section method has the largest initial support force, while the CRD method has the smallest one. It can be seen that for the CRD method, the initial support of the law is more stable. However, it can be seen from the deformation comparison diagram of the secondary lining that the CRD method has the smallest deformation value and the slowest deformation rate, while the full-section method has the largest deformation value and the fastest deformation rate. The CRD method has more advantages than the two other excavation methods in large-section deep-buried tunnels.

(3) Numerical simulation software can have certain problems, such as the real where the full-section method excavation is not possible for the V-grade surrounding rock, but in the numerical simulation, excavation can be carried out, and the corresponding excavation data are available; therefore, the simulation results of such numerical simulation software are sometimes wrong. The full-section method excavation in this paper is the numerical simulation of excavation under ideal conditions and can only be used as comparison data under ideal conditions.

(4) The stood measurement and analysis results can provide an important reference for similar projects and a basis for future numerical simulation analysis and informatization construction.

Author Contributions: Conceptualization, Y.H., C.W., H.X., T.L. and M.C.; Formal analysis, H.Z. and Y.O.; Project administration, Y.H., C.W. and H.X.; Resources, H.Z. and Y.O.; Writing—original draft, M.C., Y.H., C.W. and H.X.; Writing—review and editing, T.L., H.Z. and Y.O. All authors have read and agreed to the published version of the manuscript.

Funding: This work was financially supported by the Nation Natural Science Foundation of China under Grant No. 52004327.

Data Availability Statement: The source data can be obtained in the article.

Conflicts of Interest: The authors declare no conflict of interest.

References

1. Huang, H.; Zhou, P.; Chen, P.; Yang, J.; De-Lin, M. Theoretical research on different construction methods for double-line highway tunnel under-passing existing railway tunnel. *Railw. Stand. Des.* **2016**, *60*, 104.
2. Cui, L.; Zhang, W.; Shen, J.M.; Zheng, J. Mechanical response of deep-buried tunnels through soft and cracked rock mass under different excavation methods. *J. Civ. Eng. Manag.* **2012**. [CrossRef]
3. Wang, F.; Dongdong, M.; Yisheng, Y.; Yang, L. Numerical analysis on construction safety impact of different construction methods double arch tunnel. *Constr. Technol.* **2019**, *48*, 615–618.
4. Yu, Q.; Zhang, H.; Guo, X. Research on construction methods affecting on stress and strain distribution of double arch tunnel. *Appl. Mech. Mater.* **2013**, *256–259*, 1308–1311.
5. Zhang, Y.; Li, W.; Li, J. The tunnel of small interval clip rock mechanics properties research. *Appl. Mech. Mater.* **2012**, *170–173*, 1816–1819.
6. Wu, K.; Zheng, Q.; Shao, Z.; Zhang, Z. Research into the effect of different tunnel excavation methods on rail track settlement. *Indian Geotech. J.* **2018**, *48*, 677–685. [CrossRef]
7. Jin, H.; Yuan, D.; Zhou, S.; Zhao, D. Short-Term and Long-Term Displacement of Surface and Shield Tunnel in Soft Soil: Field Observations and Numerical Modeling. *Appl. Sci.* **2022**, *12*, 3564. [CrossRef]
8. Frough, O.; Khetwal, A.; Rostami, J. Predicting tbm utilization factor using discrete event simulation models. *Tunn. Undergr. Space Technol.* **2019**, *87*, 91–99. [CrossRef]
9. Wu, H. Numerical Simulation Algorithm Design of Influence on Existing Tunnel by Underpass Construction of New Tunnel. *Sci. Program.* **2021**, *2021*, 1734308. [CrossRef]
10. Lee, H.; Choi, H.; Choi, S.; Chang, S.; Kang, T.; Lee, C. Numerical Simulation of EPB Shield Tunnelling with TBM Operational Condition Control Using Coupled DEM–FDM. *Appl. Sci.* **2021**, *11*, 2551. [CrossRef]
11. Zhang, W.; De, C.; Liu, X.; Taerwe, L. Optimization Study on Longitudinal Joints in Quasi-Rectangular Shield Tunnels. *Appl. Sci.* **2021**, *11*, 573. [CrossRef]
12. Ngoc, A.; Dias, D. A comparison of 2D and 3D numerical simulations of tunnelling in soft soils. *Environ. Earth Sci.* **2017**, *76*, 102. [CrossRef]
13. Lu, H.; Shi, J.; Wang, Y.; Wang, R. Centrifuge modeling of tunneling-induced ground surface settlement in sand. *Undergr. Space* **2019**, *4*, 302–309. [CrossRef]
14. Lou, P.; Li, Y.; Xiao, H.; Zhang, Z.; Lu, S. Influence of Small Radius Curve Shield Tunneling on Settlement of Ground Surface and Mechanical Properties of Surrounding Rock and Segment. *Appl. Sci.* **2022**, *12*, 9119. [CrossRef]
15. Yang, C.; Chen, Y.A.; Guo, Z.; Zhu, W.; Wang, R. Surface Settlement Control in the Excavation of a Shallow Intersection between a Double-Arched Tunnel and a Connection Tunnel. *Int. J. Geomech.* **2021**, *21*, 04021035. [CrossRef]
16. Topal, C.; Mahmutolu, Y. Assessment of surface settlement induced by tunnel excavations for the Esenler–Baakehir (Istanbul, Turkey) subway line. *Environ. Earth Sci.* **2021**, *80*, 188. [CrossRef]
17. Liang, X.; Ye, F.; Ouyang, A.; Han, X.; Qin, X. Theoretical analyses of the stability of excavation face of shield tunnel in lanzhou metro crossing beneath the yellow river. *Int. J. Geomech.* **2020**, *20*, 04020200. [CrossRef]

18. Gychan, J.; Donghyun, K. A study on key factors of ground settlement due to shield tbm excavation using numerical analysis and field measurement comparison. *J. Korean Geosynth. Soc.* **2017**, *16*, 63–72. [CrossRef]
19. Dejong, M.; Giardina, G.; Chalmers, B.; Lazarus, D.; Ashworth, D.; Mair, R. The impact of the crossrail tunnelling project on masonry buildings with shallow foundations. *Proc. ICE Geotech. Eng.* **2019**, *172*, 402–416. [CrossRef]
20. Jiang, A.; Peng, L.; Shi, H. Shallow depth of the tunnel excavation response research based on crd method—Sciencedirect. *Procedia Eng.* **2011**, *15*, 4852–4856.
21. Li, X.; Wang, S.; Zhang, B.; Wang, Y.; Peng, W. Ground surface settlement prediction and reliability analysis of twin tunnels. *Chin. J. Undergr. Space Eng.* **2019**, *15*, 428–435.
22. Kim, D.; Pham, K.; Park, S.; Oh, J.; Choi, H. Determination of effective parameters on surface settlement during shield tbm. *Geomech. Eng.* **2020**, *21*, 153–164. [CrossRef]
23. Saeed, H.; Uygar, E. Equation for maximum ground surface settlement due to bored tunnelling in cohesive and cohesionless soils obtained by numerical simulations. *Arab. J. Sci. Eng.* **2022**, *47*, 5139–5165. [CrossRef]
24. Kannangara, K.; Ding, Z.; Zhou, W. Surface settlements induced by twin tunneling in silty sand. *Undergr. Space* **2021**, *7*, 58–75. [CrossRef]
25. Hsda, B.; Hlfa, B.; Shi, Y.; Zhen, H.C.; Yyza, B. Ground loss model for analyzing shield tunneling-induced surface settlement along curve sections. *Tunn. Undergr. Space Technol.* **2022**, *119*, 104250. [CrossRef]
26. Chen, Y. Discussion on construction technology of large-section stone tunnel by CD method. *Green Build. Mater.* **2021**, *2*, 121–122. [CrossRef]
27. Li, C.K. Optimization analysis of different excavation offsets in railway pilot tunnel by crd method. *Appl. Mech. Mater.* **2014**, *505–506*, 134–138.
28. Rehman, H.; Ali, W.; Naji, A.; Kim, J.; Abdullah, R.; Yoo, H. Review of Rock-Mass Rating and Tunneling Quality Index Systems for Tunnel Design: Development, Refinement, Application and Limitation. *Appl. Sci.* **2022**, *8*, 1250. [CrossRef]
29. Peck, R. Deep excavations and tunneling in soft ground. In Proceedings of the 7th International Conference on Soil Mechanics and Foundation Engineering, Mexico City, Mexico, 29 August 1969; pp. 225–290.
30. Chen, Y.; Yang, X. The decline curve shape estimate analysis of parallel tunnel surface. *Shanxi Archit.* **2009**, *35*, 338–339. [CrossRef]
31. Wu, H.; Wei, G. The calculation of soil settlement induced by construction of twin parallel shield tunnels with a small-interval. *Mod. Tunn. Technol.* **2014**, *51*, 63–69+75.
32. New, B.; Bowers, K. Ground movement model validation at the Heathrow Express trial tunnel. In *Tunnelling'94*; Springer: Boston, MA, USA, 1994. [CrossRef]